Research Article

Effect of Amorphous Silica–Forming Additive on Porosity and Mechanical Strength in Autoclaved Aerated Concrete Thermal Insulation Board

Yunus Ion Grecu[1*], Ezgi Biçer[2], Emre Fenerci[3], Ebru Erdoğan[4], Fatma Bakır[5]

[1] Nuh Yapı Ürünleri A.Ş. R&D Center, Kocaeli, Türkiye, Orcid ID: https://orcid.org/0000-0001-5034-7262, E-mail: ion.grecu@nuhyapi.com.tr
[2] Nuh Yapı Ürünleri A.Ş. R&D Center, Kocaeli, Türkiye, Orcid ID: https://orcid.org/0000-0002-8374-7796, E-mail: ezgi.bicer@nuhyapi.com.tr
[3] Nuh Yapı Ürünleri A.Ş. R&D Center, Kocaeli, Türkiye, Orcid ID: https://orcid.org/0009-0005-8160-5347, E-mail: emre.fenerci@nuhyapi.com.tr
[4] Nuh Yapı Ürünleri A.Ş. R&D Center, Kocaeli, Türkiye, Orcid ID: https://orcid.org/0009-0000-5403-5792, E-mail: ebru.erdogan@nuhyapi.com.tr
[5] Nuh Yapı Ürünleri A.Ş. R&D Center, Kocaeli, Türkiye, Orcid ID: https://orcid.org/0000-0002-1352-1126, E-mail: fatma.bakir@nuhyapi.com.tr

[*] Correspondence: ion.grecu@nuhyapi.com.tr; +905444176293

Received: 14 March 2025
Revised: 21 August 2025
2nd Revised: 25 September 2025
3rd Revised: 18 October 2025
Accepted: 06 December 2025
Published: 12 December 2025

Reference: Grecu, Y. I., Biçer, E., Fenerci, E., Erdoğan, E., & Bakır, F. (2025). Effect of amorphous silica–forming additive on porosity and mechanical strength in autoclaved aerated concrete thermal insulation board. *The European Journal of Research and Development, 5*(1), 449–464.

Abstract

Autoclaved aerated concrete (AAC) thermal insulation board has a density of 130–155 kg/m³, a compressive strength above 0.4 MPa and a thermal conductivity value of 0.045 W/m.K. It is a Class A non-combustible, mineral-based and non-toxic material and used for thermal insulation from the outside, inside, in the middle, underground, on floors, and roof surfaces. The porous structure of the material decisively affects its mechanical and thermal conductivity properties. In this study, the potential for pore size reduction was evaluated by adding ratios of 0%, 0.1%,

0.25%, 0.5%, 0.75% and 1% amorphous silica-forming additive to the AAC thermal insulation board by mass. Furthermore, the mechanical performance was compared with the corresponding pore size characteristics. In determining the pore distribution, the air pores in the structure were examined by image analysis technique based on the Monte Carlo approach. When the density and compressive strength of the samples obtained after hydrothermal curing were compared with the A value, it was observed that the highest increase was 29.94% with a 1% additive rate. Scanning electron microscope (SEM) and X-ray diffraction (XRD) analyses showed that the amount of tobermorite increased continuously up to a dosage of 0.5%. The fact that the addition of the admixture by mass reduces the pore diameter, reduces density and increases compressive strength reveals that the amorphous silica-forming additive is usable in AAC thermal insulation board. Achieving the same compressive strength with less material during the production phase and reducing per-unit energy consumption during service due to improved thermal insulation associated with smaller pore sizes are critical for lowering the carbon footprint.

Keywords: Autoclaved aerated concrete, Monte Carlo method, Chemical agent, Thermal insulation board, Tobermorite.

1. Introduction

Buildings have a significant share in total energy consumption, with a large portion of consumption occurring in heating, cooling, and ventilation processes. A properly designed thermal insulation contributes to the reduction of greenhouse gas emissions by reducing energy use in the range of 30–60% while maintaining comfort in the range of 21 ± 1°C indoors [1–5]. The performance of the insulation of the material is directly dependent on its hygrothermal behavior which is dependent on temperature and humidity. Since thermal conductivity and moisture transport differ in the transition between dry state and wet state it is important to determine the correct parameters in energy performance and material selection [6].

The approach to the thermal performance of exterior walls in Turkey has been institutionalized since the 1990s with the spread of sheathing systems and the U-value limits defined by TS 825. Over time, insulation thicknesses have increased according to climatic zones, and the control of thermal bridges such as columns, beams and lintels has come to the fore in application details. With the right thermal insulation, the transfer of heat from the inner volume to the outer shell is reduced in winter while both comfort and heating/cooling balance are optimized by limiting the transfer of external heat inside in summer [1,3,7].

In the selection of thermal insulation materials, the thermal conductivity coefficient (λ) is expected to be low. The fact that it is at a temperature of 23°C under 80% relative humidity conditions and that the thermal conductivity coefficient is lower than 0.065 W/m.K is a reference for the acceptance of products as insulation materials [1,2,8]. Water

vapor diffusion resistance (μ), fire behavior and toxicity, water absorption by volume, economic and ecological indicators are among the parameters to be considered in the materials to be used in insulation. Lightness is at the forefront in terms of seismic activity [3,8–10].

Autoclaved aerated concrete thermal insulation board is characterized by the formation of a stable skeleton of tobermorite as a result of the transformation of calcium-silicate-hydrate (C-S-H) phases in the autoclave cure, of the pores formed as a result of mixing and swelling of the lime-cement-quartzite based mixture by blending it with aluminum powder additive. In the microstructure, C-S-H gel phases and tobermorite crystals are found together with bridges that provide charge transfer between air-filled spaces. Dry unit weight and moisture content affect thermal conductivity. The porous structure, which affects the dry unit weight, makes the material a good insulator thanks to the air-filled voids that limit heat transfer. For AAC thermal insulation boards in the insulation class, which are not load-bearing and used to increase the thermal efficiency of the wall for insulation purposes, dry density is used in the range of 85–155 kg/m^3 and thermal conductivity value is used between 0.042–0.047 W/m.K [11–14]. Although increasing the porosity rate contributes to sound damping, diffusion, and capillary activity should be considered in terms of hygrothermal behavior. Water vapor produced indoors can cause condensation that poses a risk in terms of strength and durability by moving through the section with the pressure difference. Diffusion-open but controlled and at the same time capillary-active mineral systems limit the penetration of condensate into the wall that may form in the interlayer, carry moisture to the inner surface and remove it by evaporation [1,4,11].

In the mechanical behavior of AAC thermal insulation board, 11 Å tobermorite formed under autoclave conditions strengthens the solid skeleton and supports compressive strength and thermal performance. Tobermorite formation occurs in the CaO-SiO_2-H_2O system by a chemical reaction proceeding at a certain pH, temperature, and CaO/SiO_2 ratio [15,16]. The reactivity of the silica source affects the formation of tobermorite. Amorphous silica dissolves faster than its crystalline state and promotes the formation of C-S-H by enriching the solution in Si^{4+}, facilitating the formation of more tobermorite crystals [16,17]. In studies on AAC structures with amorphous silica in the literature, Hust'avova et al. [18] added amorphous glass instead of silica sand at substitution rates of up to 100% and found 25% amorphous glass substitute as the optimum level in compressive strength. Shams et al. [19] changed the CaO/SiO_2 ratio by using calcined diatomite instead of silica sand and stated in their study that tobermorite formation was encouraged at lower autoclave temperatures and increased compressive strength by 30%. In another study by Shams et al. [20], they observed the formation of more tobermorite with a 22% increase in compressive strength at lower than normal autoclave temperatures by using rice husk ash instead of silica sand. Corro-Escorcia et al. [21] showed that the

addition of diatomite instead of silica sand increased the formation of 11 Å tobermorite from 17.2% to 38%.

The targeted design in AAC thermal insulation board is to maintain mechanical stability while thermal conductivity decreases. In this context, pore size distribution and geometry are primary importance. Balanced and multi-distributed pore architecture both reduces heat conduction and can create a solid matrix that will not interrupt charge transfer paths [12,23].

The aim of this study is to systematically investigate how varying ratios of amorphous silica-forming chemical additive affects the pore architecture, microstructure, density, and mechanical performance of AAC thermal insulation board.

2. Experimental Setup and Method

2.1. Sample Preparation

Quartz sand, cement, lime, and water are used as the basic raw materials to produce the AAC thermal insulation board, while aluminum powder is used as a foaming agent. Admixture of R was selected as an amorphous silica-forming additive and crystalline silica to represent quartz sand. Lime was used to increase the calcium oxide content in the mixture, cement to provide setting and ultimate strength, and gypsum to provide setting balance. R admixture is a consolidant that is colorless and could form a silicate network.

Table 1: Prepared sample compositions

Group	Description
R0	Lime, quartz sand, cement, gypsum, water, aluminum powder (AAC insulation board receipt)
R1	+R 0.1% of total weight
R2	+R 0.25% of total weight
R3	+R 0.5% of total weight
R4	+R 0.75% of total weight
R5	+R 1% of total weight

The density of the AAC thermal insulation board used in the study is 145–155 kg/m^3 and the compressive strength is 0.5> MPa a mix-design has been prepared to be produced. In Table 1, the total solid is added as 0%, 0.1%, 0.25%, 0.5%, 0.75% and 1% in the recipe prepared with admixture of R and named as R0, R1, R2, R3, R4, R5, respectively.
As shown in Figure 1, sample preparation involves mixing water and admixture of R for 120 seconds to ensure a homogeneous distribution, followed by mixing the mixture of

quartz sand, cement, lime, and gypsum with R-containing water for another 120 seconds. As a result of mixing, aluminum powder is added to the fresh mixture to initiate the foaming reactions, mixed for another 40 seconds, poured into the mold and left at 50°C for 24 hours to set and remove from the mold. The green cake, which has reached the hardness that can be removed from the mold, is hydrothermally cured for 12 hours at 190°C under a pressure of 1.2 MPa in autoclave, resulting in an AAC thermal insulation board product.

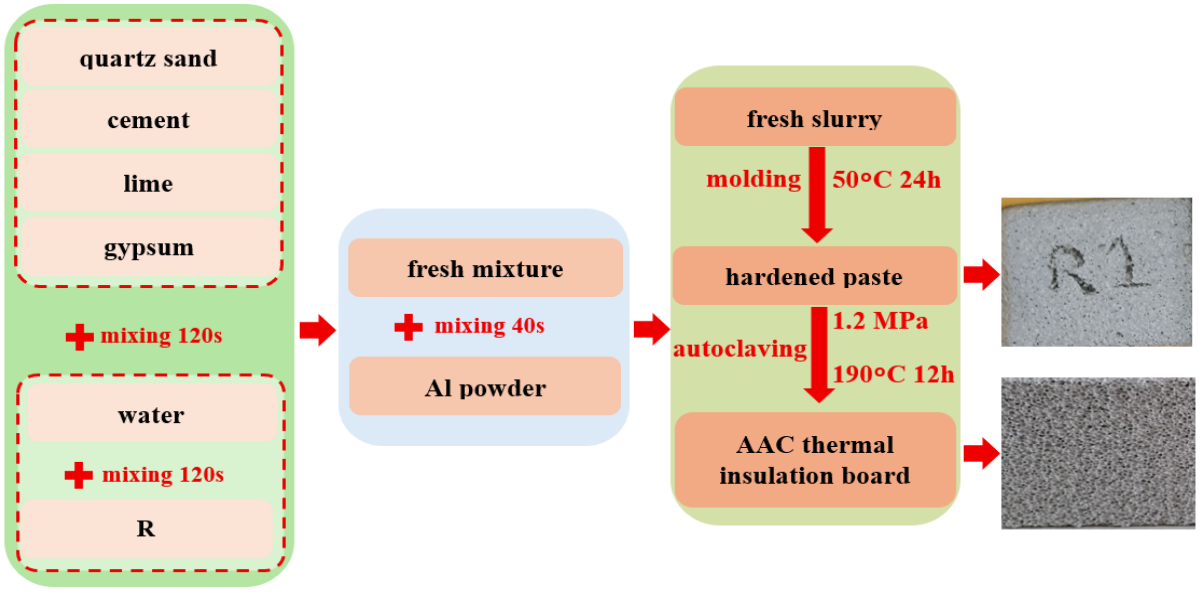

Figure 1: Preparation flow chart of AAC insulation board samples incorporated with R

2.2. Test Procedure

2.2.1. Dry Density

The density of the samples has been calculated according to the criteria specified in TS EN 772-13 and TS EN 772-14 standards. After curing in the autoclave, three samples with dimensions of 50 mm x 50 mm x 50 mm are kept in the oven for 24 hours at a temperature range of 105 ± 5°C until the sample reaches a constant mass and the dry density is calculated.

2.2.2. Compressive Strength

The compressive strength of the sample is made by cutting three samples in 100 mm x 100 mm x 100 mm dimensions after curing in autoclave according to TS EN 772-1 and TS EN 771-4 standards and applying the mechanical test when the moisture content reaches 3–6% in the temperature range of 60 ± 5°C. Dinç Machine D201.A device was carried out for compressive strength test.

2.2.3. A Value

A value was developed for the comparison of density and compressive strength in AAC thermal insulation board. A value is given in Equation 1, the experimentally verified potential function of the relationship between compressive strength and density.

$$\text{A Value} = \frac{\sigma}{0.016 \times \rho^2} \quad (1)$$

Here, σ represents the compressive strength (N/mm^2), ρ represents the density (kg/m^3) and the value 0.016 represents a constant number.

2.2.4. Air Pore Structure

When the image of the AAC thermal insulation board obtained with the camera is in color, each pixel is represented by three two-dimensional arrays of similar size and each of which corresponds to one of the primary color components. Since color type of image data contains high information, the analysis and processing stages become more demanding. The image is expressed with a two-dimensional array at the gray level, simplifying the amount of data and separating the color depth between black and white, increasing the accuracy of the analysis [22,23].

A series of image processing and analysis steps were applied using ImageJ software to examine the pore structure in the AAC thermal insulation board. Images for the camera have been acquired from a fixed distance in the direction of the swell to ensure consistency of pixel size and resolution. Figure 2 shows samples of AAC thermal insulation board containing admixture of R in different proportions cropped to 490 pixels x 490 pixels size.

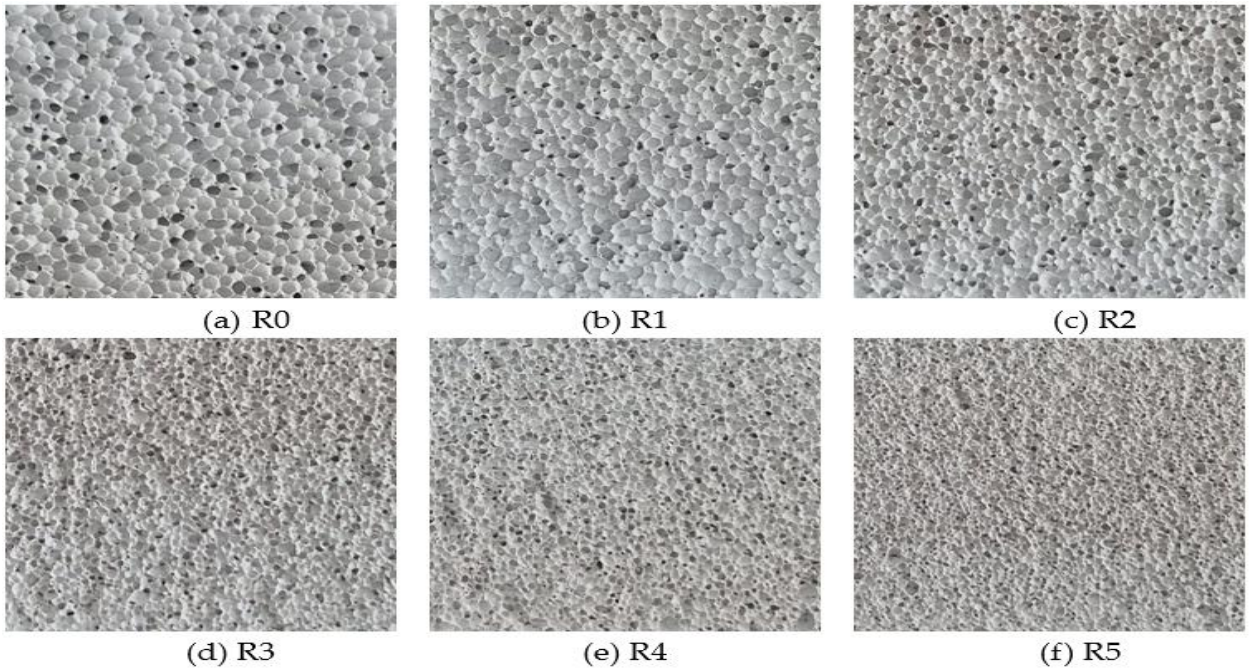

Figure 2: Images of AAC thermal insulation board with varying admixture of R, acquired along the expansion direction and cropped to 490 x 490 pixels: (a) 0%, (b) 0.1%, (c) 0.25%, (d) 0.50%, (e) 0.75%, (f) 1%

Processing raw image data in the preprocessing phase consists of a series of steps. The first step is to convert the image to 8-bit grayscale format, simplifying the color information and reducing the complexity of the image data. Next, the median filter is a filter that sorts the image edges while preserving them. Noise reduction is made with the smoothing filter, reducing high-frequency variations and softening the image. After noise reduction, Otsu's global threshold was employed to separate the pores from the surrounding solid matrix.

Following threshold process, the watershed algorithm was used to determine the boundaries by dividing the pore regions into single-pore discrete regions. Subsequently, each pore was defined separately, and the pore distribution was determined with the Monte Carlo method in Python software. The results for the AAC thermal insulation board images were converted from color format to gray format for pore detection are shown in Figure 3 (a-f).

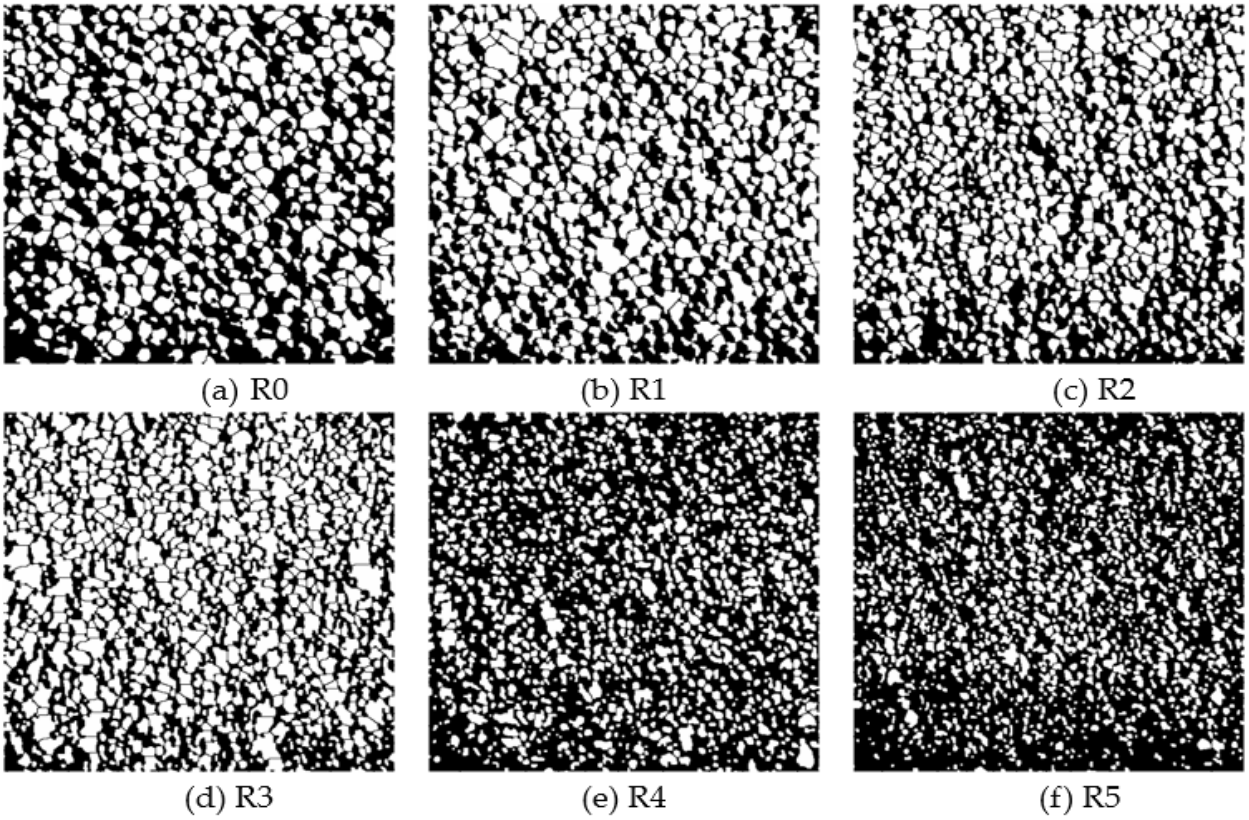

Figure 3: Results obtained via threshold analysis of the images

2.2.5. Characterization of Cured Products

X-ray diffractometer (XRD, Rigaku, Sakarya University) using Cu-Kα radiation was used to observe the mineral phase change of powder samples containing different proportions of chemicals after curing in the autoclave. The measurement parameters are set at 2θ range 5°–60°, scanning speed 5°/min, voltage 40 kV and current 30 mA. The microstructure and morphology of the final products were examined with a scanning electron microscope (SEM, Hitachi SU7000, Diler Demir Çelik Endüstri & Tic. A.Ş). Before the SEM test, samples cut in 10 mm x 10 mm x 10 mm dimensions were dried in an oven and then coated with gold.

3. Results and Discussion

Density and compressive strength are important parameters in determining the characteristics of AAC thermal insulation board. The compressive strength needs to be analyzed together with the density. Figure 4 shows the change in density and compressive strength of AAC thermal insulation board with increasing R.

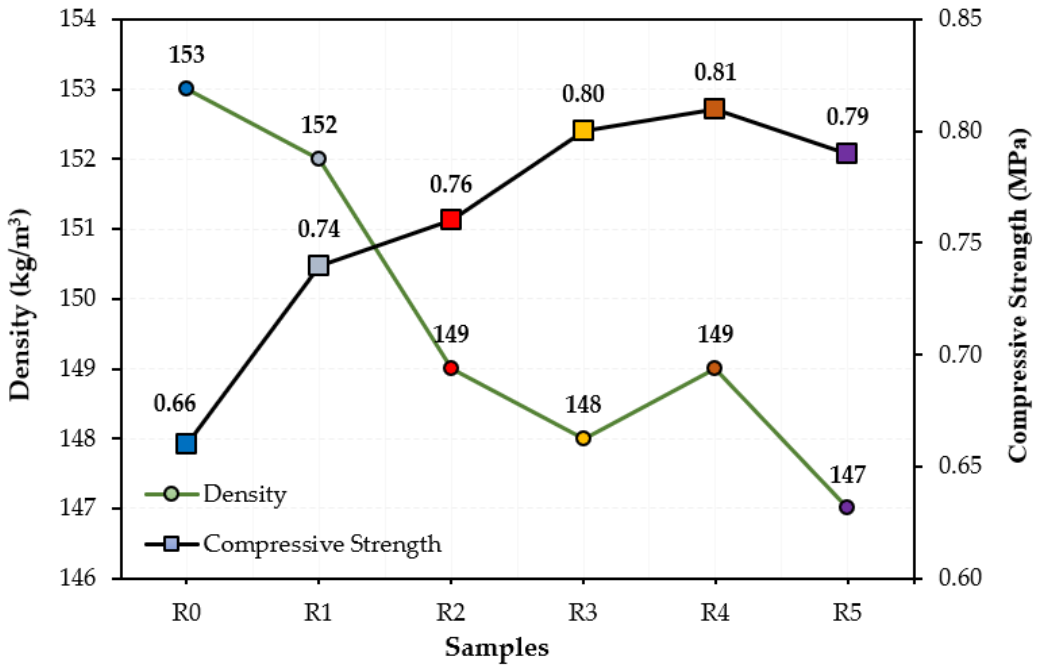

Figure 4: Effect of adding R to AAC thermal insulation board on density and compressive strength

In the recipe of AAC thermal insulation board, adding R to the total solid reduces the density up to the R3 sample. The increase in R4 was seen as a decrease in R5 again. The R5 sample has the lowest density of 147 kg/m^3 and is 6 kg/m^3 lower than the R0 sample. As the addition rate of R increases, there is a tendency to increase in compressive strength up to R4 and then decrease. While the addition rate of R was in the range of 0–0.75%, a linear increase in compressive strength was achieved. Compared to the R0 sample, the compressive strength of R1, R2, R3, R4, and R5 samples are higher by 0.08 MPa, 0.10 MPa, 0.14 MPa, 0.14 MPa, and 0.13 MPa respectively. The compressive strength increase of up to 21.83%, concomitant with a 3.69% decrease in density, is attributed to the enhanced formation of R-induced hydration products and is therefore considered the primary cause of the observed gain strength.

The compressive strength of AAC thermal insulation board depends on both the pore structure and hydration products. Correlation between compressive strength and density are shown in Figure 5. With the proportional increase in the amount of R from R0 to R3, an increasing slope in the A value was observed at the same time. Compared to the R0, the A value of the R1, R2, R3, R4, and R5 are higher by 243, 376, 521, 520, and 527 respectively. The highest increase was seen in the R5 sample with a rate of 29.94%. Since the A values of the R3, R4 and R5 samples are close to each other, it has been determined that the ideal ratio that can be used is the R3 sample, which provides a 29.6% increase compared to R0.

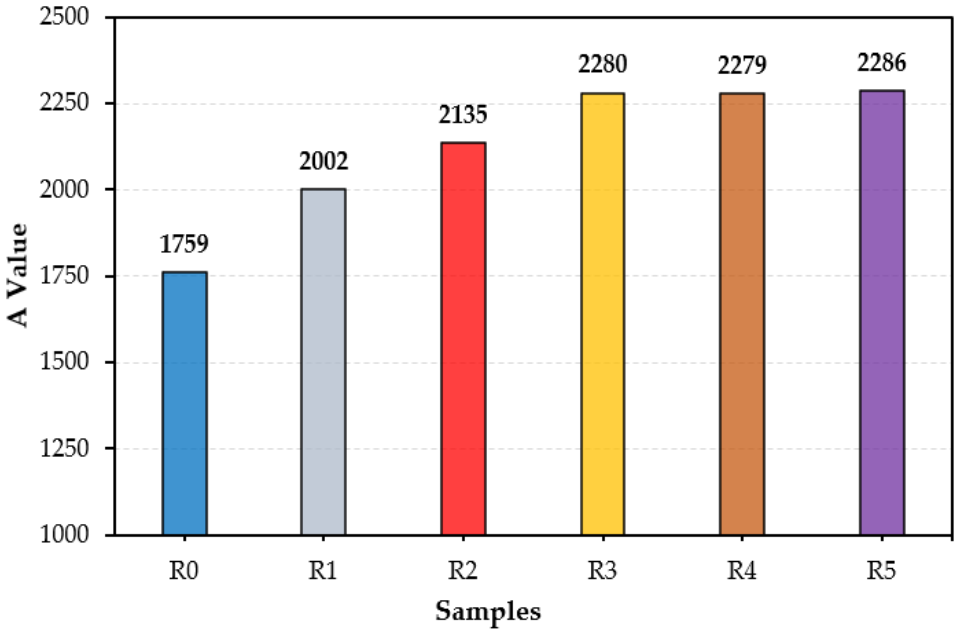

Figure 5: The effect of adding R to AAC thermal insulation board on the A Value

Based on the outcomes of the image processing process the Monte Carlo method was used in Python software to determine the pores of 50 mm x 50 mm AAC thermal insulation board with an area of 490 pixels x 490 pixels. The pore fractions obtained by counting the pores of two-dimensional images are given in Table 2. The numerical distribution of pore diameters is set to be 0.1–0.5 mm, 0.5–1 mm, 1–1.5 mm, 1.5–2 mm, 2–2.5 mm, and > 2.5 mm.

When the pores of the AAC thermal insulation boards were examined the pores were in the range of 0.5–1.5 mm at a rate of 75–90%. In samples such as R0, R4 and R5, the larger pore sizes are expected to decrease in thermal conductivity while in R1 and R3 the narrower distribution skewed toward smaller pores retain the solid skeleton more compact.

Table 2: Distribution statistics of pore sizes

Sample		**Pore Diameter, mm**					
		0.1 – 0.5	**0.5 – 1**	**1 – 1.5**	**1.5 – 2**	**2 – 2.5**	**> 2.5**
R0	Proportion of pores, %	12.62	37.87	36.07	10.82	2.13	0.49
R1		6.15	42.37	39.70	10.78	1.00	0
R2		7.79	40.52	39.22	11.69	0.78	0
R3		5.24	36.65	52.36	5.24	0.52	0
R4		10.41	37.66	42.08	8.56	1.28	0
R5		8.00	40.17	42.50	8.50	0.83	0

XRD patterns and quantitative XRD (QXRD) results of AAC thermal insulation boards with admixture of R ranging from 0–1% are presented in Figure 6 and Figure 7. The most dominant phase among the reaction products developed after hydrothermal curing was determined as 11 Å tobermorite. Tobermorite 11 Å at 7.8°, 29°, and 49.3° at positions 2θ; quartz at 27°, 39.7°, and 49.8°; hydroxylellastadite at 32.7°, and 49°; calcite at 29.1°, 43.4°, and 47.6°; belite at 31.9°, and 32.7°; anhydride at 25.5°, and 31.4°; at 17.7°, and 34° reflections of the portlandite phases were observed.

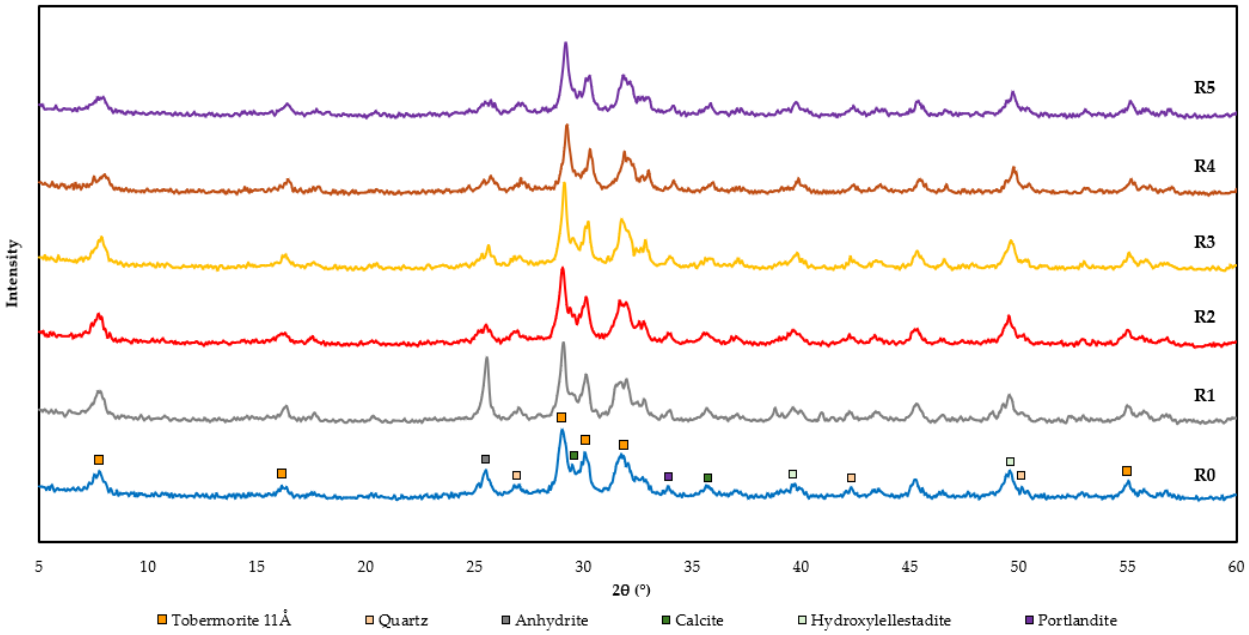

Figure 6: XRD patterns of AAC thermal insulation board specimens with varying R contents

The QXRD results in Figure 7 show that at an admixture R of 0.5%, the tobermorite diffraction peak intensity attains a maximum and then exhibits an approximately linear decline with further additions. In this case, the percentage of tobermorite increased from 40.0% to 43.8% while the amorphous fraction decreased from 22.3% to 16.9%. The increase in tobermorite was accompanied by a simultaneous decrease in the amount of calcite and amorphous phases.

Upon examination of the diffraction patterns the highest and sharpest XRD peaks were observed for the tobermorite phase. An increase in the intensity and the amount of the tobermorite phase in the matrix also increases the compressive strength from mechanical properties. R3 contains the highest amounts of tobermorite with 43.8%.

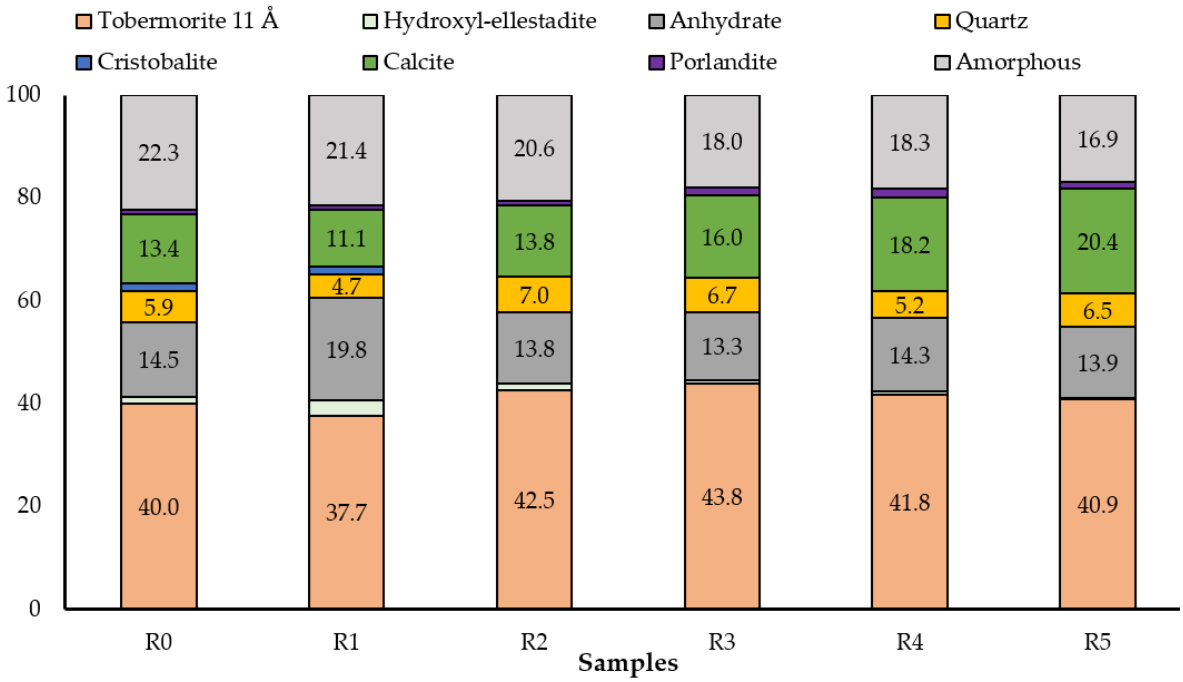

Figure 7: QXRD analysis of samples with varying R dosage (wt. %)

The morphology of the phases in the AAC thermal insulation board was examined by SEM. Figure 8 shows the phase morphology of the samples produced with R increasing from 0% to 1%. Figure 8a depicts the morphology of the sample without R and the dominant portlandite by volume was seen in the structure next to the needle-/lath-like tobermorite. During hydrothermal curing portlandite reacts with dissolved SiO_2 to form the tobermorite.

In Figure 8b-c, the amorphous calcium-silicate-hydrate (C-S-H) and the needle-/lath-like tobermorite are in the foreground. As indicated in Equation 2, the amorphous C-S-H enable the formation of the tobermorite prior to hydrothermal curing. An increase in the C-S-H indicates that the conversion to tobermorite is low.

$$3Ca(OH)_2 + 2SiO_2 \rightarrow \text{C-S-H} \quad (2)$$

Across Figures 8d–f, the effect of the R leads to partial coating and improved reaction within the matrix. Consequently, the tobermorite is refined and the pore sizes are reduced, which is consistent with the observed increase in compressive strength. In Equations 3 and 4, the formation reactions of the tobermorite are given.

$$5Ca(OH)_2 + 6SiO_2 \rightarrow C_5S_6H_5 \quad (3)$$

$$\text{C-S-H} + SiO_2 \rightarrow C_5S_6H_5 \quad (4)$$

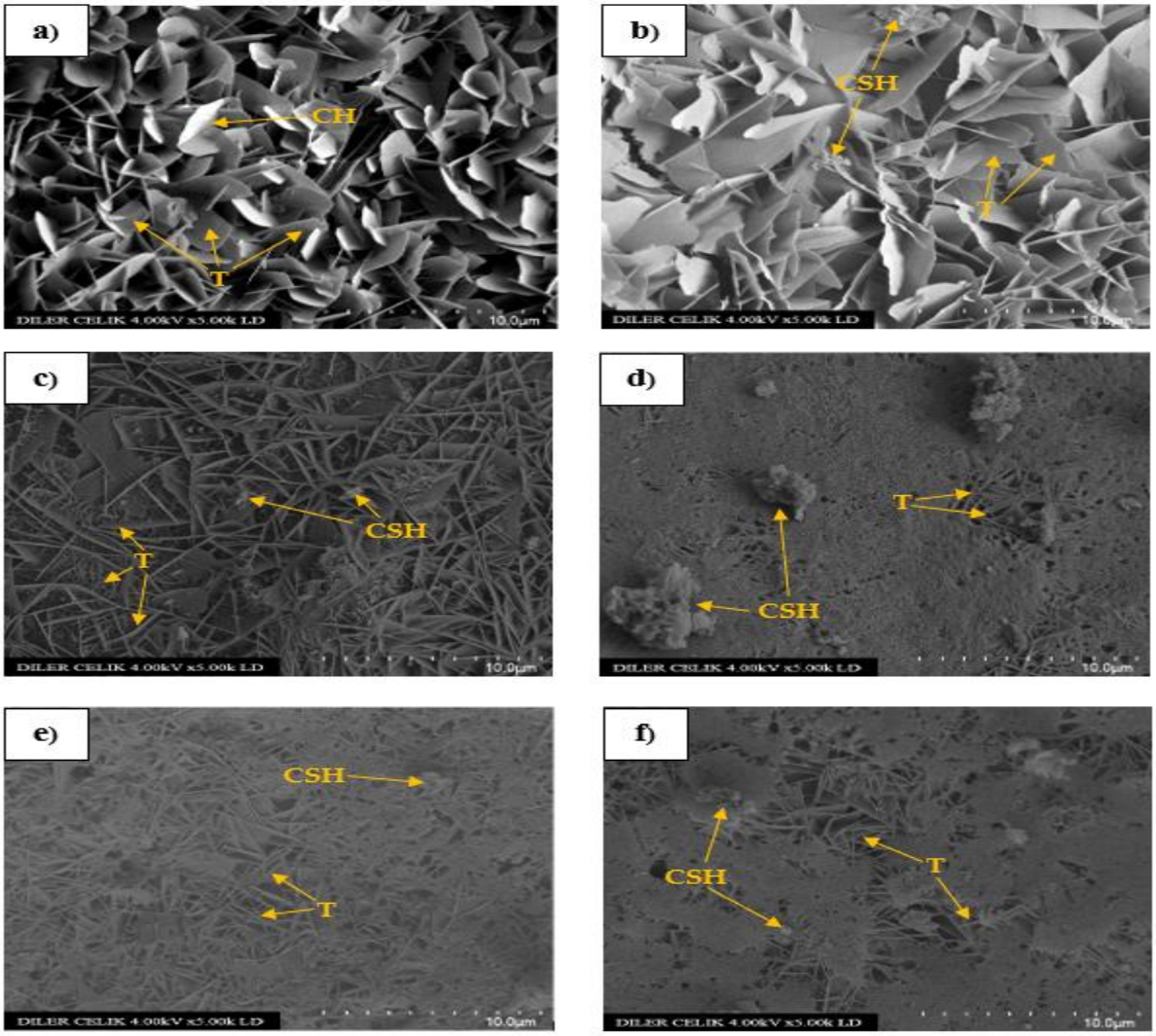

Figure 8: SEM images of AAC thermal insulation board samples containing R in various proportions at 5000x magnification (a) R0, (b) R1, (c) R2, (d) R3, (e) R4, (f) R5 (CH: portlandite, CSH: Calcium-silicate-hydrate, T: Tobermorite)

4. Conclusion

This study examines the effects of chemical admixture added in different proportions during the production process on the mechanical behavior and pore distribution of AAC thermal insulation board. Density, compressive strength, and A value properties were compared with experimental methods; pore morphology was evaluated with an image analysis considering the direction of foaming. As a result of the addition of R admixture in the range of 0-1%:

1) In compressive strength tests on 100 mm × 100 mm × 100 mm cubes with loading applied opposite to the expansion direction, the maximum increase with 22.72% was

achieved at R dosage of 0.75%. The largest increase in the A value was 29.94%, observed at dosage of 1%.

2) The pore distribution from the cross-sectional images was determined based on the Monte Carlo approach. The analysis volume employed was 50 mm × 50 mm. When the pores in the <1.5 mm range were examined, the maximum fraction with 94.25% was observed at R dosage of 0.5%.

3) According to XRD/QXRD analysis, applying R dosage of 0.5% maximized the formation of 11 Å tobermorite to 43.8%, thereby reducing the amorphous/calcite and increasing compressive strength. It was determined that tobermorite density decreases linearly at higher dosage rate.

4) SEM analyses showed that portlandite and C-S-H were significantly dominant in volume in the non-additive sample and at the dosage range of 0.1–0.25%. It has been shown that these phases decrease by increasing the R ratio to 0.5% and above, and a coating layer is formed on the surface with the effect of the admixture. As a concomitant effect, size reduction was observed in the needle-/lath-like tobermorite phase.

In conclusion, although R dosages of 0.5%, 0.75%, and 1% are all suitable for use the obtained A values are close to each other. At 0.5%, the A value reached 2280, with an increase of 29.62% and moreover, because the proportion of pores < 1.5 mm was 94.25%, this dosage was identified as the optimum for practical application.

Through mix-design optimization, material savings are achieved without decreasing compressive strength and the process energy load is reduced. Also the improved thermal insulation arising from smaller pore sizes limits heat losses through the building, thereby reducing CO_2 emissions.

5. Acknowledge

This study is based on the results obtained under the project “Enhancing the Mechanical Fracture Strength of the Thermal Insulation Board” conducted by the Nuh Yapı Ürünleri A.Ş. R&D Center.

References

[1] Özgür, Y., Özkan Ş., Haluk, Ş., Osman, Ç., Demet, Ö., Şükrü, E. & İlkay, K. (2015). Binalarda ısı yalıtımı ve ısı yalıtım malzemeleri. IMO Yapı Malzemeleri Komisyonu, 60, 62-73.

[2] Bayraktar, D. & Bayraktar E. A. (2016). Mevcut binalarda ısı yalıtım uygulamalarının değerlendirilmesi. Mehmet Akif Ersoy Üniversitesi Fen Bilimleri Dergisi, 7, 59-66.

[3] Bektaş, V., Çerçevik, A. E. & Yerel Kandemir, S. (2017). Binalarda ısı yalıtımının önemi ve ısı yalıtım malzemesi kalınlığının yalıtıma etkisi. Bilecik Şeyh Edebali Üniversitesi Fen Bilimleri Dergisi, 4, 36-42.

[4] Zhao, J., Grunewald, J., Ruisinger, U. & Feng, S. (2017). Evaluation of capillary-active mineral insulation systems for interior retrofit solution. Building and Environment, 115, 215-227.

[5] Akdemir, Ö., Hacırecepoğlu, A., Andıç Çakır, Ö., Sarıkanat, M., Sever, K. & Seki, Y. (2020). Poliüretanın ısı yalıtım özelliklerinin silika esaslı partiküllerle iyileştirilmesi. Dokuz Eylül Üniversitesi Mühendislik Fakültesi Fen ve Mühendislik Dergisi, 22(64), 147-153.

[6] Jerman, M. & Cerny, R. (2012). Effect of moisture content on heat and moisture transport and storage properties of thermal insulation materials. Energy and Buildings, 59, 39-46.

[7] Kotan, T., Fırat, I, Kaya, M. & Ulusu, I. (2018). Binalarda kullanılan farklı ısı yalıtım malzemelerinin ısı iletkenlik katsayılarının Erzincan ili şartlarında termokupl ve termal kamera ile incelenmesi. Uludağ Üniversitesi Mühendislik Fakültesi Dergisi, 23(2), 367-382.

[8] Gören, B. (2022). Gazbeton ısı yalıtım levhasının taş yünü ısı yalıtım malzemesi ile karşılaştırılarak bina enerji performansı ve ısınma maliyetine etkisinin incelenmesi. İstanbul Arel Üniversitesi, Lisansüstü Eğitim Enstitüsü.

[9] Karadayı, T. T. & Yüksek, I. (2016). Yapılarda ısı yalıtım malzemeleri seçimi üzerine bir araştırma. Tesisat Dergisi, 242, 90-102.

[10] Arslan, A. M. & Aktaş, M. (2018). İnşaat sektöründe kullanılan yalıtım malzemelerinin ısı ve ses yalıtımı açısından değerlendirilmesi. Journal of Polytechnic, 21(2), 299-320.

[11] Kreft, O., Straube, B. & Torsten, S. (2011). Internal thermal insulation with light weight autoclaved aerated concrete. In Proceedings of the International Autoclaved Aerated Concrete Conference, Bydgoszcz.

[12] Miccoli, L., Fontana, P., Silva, N., Kocadag, R., Cederqvist, C., Kreft, O. & Ovaeschning, D. (2016). UHPC-AAC/CLC composite panels with self-cleaning properties. Materials and Production Technology.

[13] Majerek, D., Sedzielewska, E., Pasnikowska-Lukaszuk, M., Lazuka, E., Suchorab, Z. & Lagod, G. (2024). Automatic image analysis method as a tool to evaluate the anisotropy of autoclaved aerated concrete for moisture and heat transport. Materials, 17, 4903.

[14] Chen, J., Huang, Y., Lie, G., Chen, H., Liang, Y., Rashad, A. M., Lie, J., Zhang, J. & Wang, W. (2025). Performance regulation of ultra-lightweight autoclaved aerated concrete by metakaolin and its impact on energy efficiency in thermal insulation walls. Energy and Buildings, 348, 116374.

[15] Galvankova, L., Masilko, J., Solny, T. & Stepankova, E. (2016). Tobermorite synthesis under hydrothermal conditions. Procedia Engineering, 151, 100-107.

[16] Cerny, V. & Drochytka, R. (2019). The influence of different types of siliceous raw materials on tobermorite formation in lime-silica composite. WSEAS transactions on environment and development, 15, 57-64.

[17] Kreft, O., Hausmann, J., Hubalkova, J., Aneziris, C. G., Straube, B. & Schoch, T. (2011). Pore size distribution effects on the thermal conductivity of light weight autoclaved aerated concrete. Cement Wapno Beton, 49-52.

[18] Hust'avova, J., Cerny, V. & Drochytka, R. (2020). Monitoring the effect of quartz-sand replacement by amorphous-silica raw material on the microstructure of calcium silicate composites. Materials and Technologies, 54(1), 129-134.

[19] Shams, T., Schober, G., Heinz, D. & Seifert, S. (2021). Production of autoclaved aerated concrete with silica raw materials of a higher solubility than quarts part II: Influence of autoclaving temperature. Construction and Building Materials, 287, 123072.

[20] Shams, T., Schober, G., Heinz, D. & Seifert, S. (2022). Rice husk ash as a silica source for the production of autoclaved aerated concrete – A chance to save energy and primary resources. Journal of Building Engineering, 47, 104810.

[21] Corro-Escorcia, I. A., Hernandez-Avila, J., Cerecedo-Saenz, E. Barrientos-Hernandez, F. R., Cruz-Hernandez, M., Toro, N., Galvez, E., Gutierrez-Amador, M. P. & Salinas-Rodriguez, E. (2025). Synthesis of tobermorite 11 A during the formation of autoclaved aerated concrete with the addition of diatomite. Results in Materials, 26, 100725.

[22] Chen, G., Li, F., Geng, J., Jing, P. & Si, Z. (2021). Identification, generation of autoclaved aerated concrete pore structure and simulation of its influence on thermal conductivity. Construction and Building Materials, 291, 123572.

[23] Uluer, O., Karaağaç, I., Aktaş, M., Durmuş, G., Ağbulut, Ü., Khanları, A. & Çelik, D. N. (2018). Genleştirilmiş perlitin ısı yalıtım teknolojilerinde kullanılabilirliğinin incelenmesi. Pamukkale Üniversitesi Mühendislik Bilimleri Dergisi, 24(1), 24-32.